Title
ATOMIC COLT.ISIONS WITH RELATIVISTIC HEAVY IONS IV: PROJECTILE K-SHELL IONIZATION

Author
Anholt, R.

Publication Date
1985-07-01

Lawrence Berkeley Laboratory
UNIVERSITY OF CALIFORNIA

Submitted to Physical Review A

ATOMIC COLLISIONS WITH RELATIVISTIC HEAVY IONS IV: PROJECTILE K-SHELL IONIZATION

R. Anholt, W.E. Meyerhof, H. Gould, Ch. Munger, J. Alonso, P. Thieberger, and H.E. Wegner

July 1985

NUCLEAR SCIENCE DIVISION

Prepared for the U.S. Department of Energy under Contract DE-AC03-76SF00098

DISCLAIMER

Atomic Collisions with Relativistic Heavy Ions IV: Projectile K-shell Ionization

R.Anholt, W.E. Meyerhof

Department of Physics, Stanford University, Stanford California 94305

H. Gould and Ch. Munger

Materials and Molecular Research Division, Lawrence Berkeley Laboratory, University of California, Berkeley, California 94720

J. Alonso

Accelerator and Fusion Division, Lawrence Berkeley Laboratory, University of California, Berkeley, California 94720

P. Thieberger and H. E. Wegner

Department of Physics, Brookhaven National Laboratory, Upton, N.Y. 11973

Abstract

Projectile 1s-ionization cross sections are reported for 82-, 140-, and 200-MeV/amu Xe projectiles incident on a variety of thin solid targets between Be and Au. The cross sections were calculated with the plane-wave Born approximation. Possible relativistic wave-function, target-screening, and transverse-excitation effects are discussed. Comparisons of the data with the perturbed stationary-state theory of Basbas et al. and the Glauber approximation are made. Scaled, interpolated Xe+Xe ionization cross sections agree well with measured p+H ionization cross sections.

I. INTRODUCTION

The present paper returns to a question considered in the first part of this series of papers on relativistic heavy-ion-atom collisions: inner-shell ionization.[1] While part I considered target inner-shell vacancy production, signaled by the emission of target K x-rays, here we consider projectile K-shell ionization, manifested by the charge-state gain by one- or two-electron heavy ions passing through thin foils. Heavy ($Z \geq 30$), relativistic one- or two-electron ions are normally in their ground 1s or $1s^2$ states. Hence, a measurement of the fraction of zero- or one-electron ions after passage through a thin foil represents a measurement of projectile 1s ionization.

The experimental arrangement is described in paper III of this series.[2] Section II of the present paper discusses the differences between studies of target K-shell ionization by measuring target K x-rays,[1] and of projectile ionization in light and heavy projectiles by measuring charge states.

Ionization cross sections can be calculated with the plane-wave Born approximation[3-5] if the ratio of the ion velocity v to the velocity v_K of the K electron being ionized is much larger than unity. This is certainly valid for the low-Z relativistic projectiles considered in paper II,[6] but is less valid for the high-Z, 82- to 200-MeV/amu Xe ions considered here, for which v/v_K is between 1 and 2. Although several minor effects are discussed in Section II, the major effect at these velocities is the binding[7] or polarization[8] of the active electron by the perturbing nucleus. The theory of these effects formulated by Basbas and co-workers[9] has been widely applied to measurements of inner-shell vacancy production. The reduction of the ionization cross sections due to the increased binding of the 1s electron in low-velocity collisions, especially where molecular orbitals are formed, has been established

clearly.[10] The polarization of the electronic wave functions brings the inner-shell electrons closer to the perturbing nucleus, which increases the excitation probability.[8] Although the polarization effect on electronic stopping powers (dominated by outer-shell target electron ionization processes) is well established, that on K-shell ionization is not as well understood. At the medium electron velocities ($v \approx v_K$) where the polarization effect should be dominant, a competing process due to the capture of target K electrons by the projectile ion obscures the increase in the cross section due to the polarization effect, if target K-shell ionization is studied.[11] The advantage of studying projectile ionization is that the equivalent process (capture of a projectile K-electron by the target) is absent due to the lack of vacancies in the target atom.

The measured cross sections are compared with theories of K-shell ionization including binding and polarization effects in Sect. III. We also make comparisons with theories that have been applied to symmetric p+H collisions. Since we have new measurements of equilibrium projectile charge states,[2] and a theory of target K-electron capture for relativistic heavy ions has now been formulated,[12] we return to the question of target K-electron capture contributions to target inner-shell vacancy production, which was left open in paper I. A difference between the relative importance of the binding and polarization effects in target ionization and in projectile ionization is suggested by the present data, but the uncertainities due to target electron capture do not allow us to draw a definite conclusion.

Evidence is obtained in this work for single-electron ionization in the collisions (T = target)

$$Xe^{53+}(1s) + T \rightarrow Xe^{54+} + T,$$

$$Xe^{52+}\ (1s^2) + T \rightarrow Xe^{53+} + T, \tag{1}$$

and for double-electron ionization:

$$Xe^{52+}\ (1s^2) + T \rightarrow Xe^{54+} + T. \tag{2}$$

We show in Sect. III.C that the double-ionization cross section can be calculated from the product of one-electron ionization probabilities[13,14] integrated over impact parameters.

II. THEORIES OF INNER-SHELL IONIZATION

A. The Plane-Wave Born Approximation

Our discussion of theories of inner-shell ionization by relativistic projectiles will contrast effects on target inner-shell vacancy production with effects on projectile ionization in low-Z and high-Z projectiles, which are summarized in Table 1. The starting point for all three is the nonrelativistic plane wave Born approximation (PWBA) in which the ionization cross section is calculated using[15]

$$\sigma_{1s} = \frac{4\pi a_0^2 Z_X^2 \alpha^2}{\beta^2} \int_0^\infty d\varepsilon \int_{q_0}^\infty \frac{dq}{q^3} |F(q)|^2. \tag{3}$$

Here, Z_X is the atomic number of the perturbing nucleus (the projectile charge for target ionization or the target charge for projectile ionization), $v = \beta c$ is the ion velocity, α is the fine-structure constant, a_0 is the Bohr radius, ε is the kinetic energy of the ionized electron, $q_0 = (E_K + \varepsilon)/v$ is the minimum momentum transfer needed to ionize the electron, E_K is the K electron binding energy, F(q) is the ionization form factor given by

$$F(q) = \langle \varepsilon | \exp(i\mathbf{q}\cdot\mathbf{r}) | 1s \rangle, \tag{4}$$

and $|\varepsilon\rangle$ and $|1s\rangle$ are continuum and 1s electronic wave functions. We shall consistently calculate single-ionization cross sections per K electron in this paper. Target K-vacancy production cross sections are defined per atom, hence are factors of two larger.[3,4]

B. Wave Function Effects

The form factor F(q) is usually calculated with nonrelativistic, hydrogenic 1s and continuum wave functions. For target K-vacancy production in neutral target atoms, one must approximate the many-electron wave functions by using a reduced effective target charge $Z^* = Z_t - 0.3$ for the K shell,[15] and one accounts for the difference between the ideal hydrogenic binding energy $\frac{1}{2} Z^{*2}$ a.u. and the actual one E_K by introducing a parameter θ_K, which is the ratio between the two. Then the ionization cross section is given by[3]

$$\sigma_{1s} = 4\pi \left(\frac{a_o \alpha Z_x}{\beta Z^*}\right)^2 f(\eta_K, \theta_K), \tag{5}$$

where $\eta_K = \beta^2/(\alpha Z^*)^2$,

$$f(\eta_K, \theta_K) = \int_{\theta_K}^{\infty} dW \int_{Q_o}^{\infty} \frac{dQ}{Q^2} |F_K(Q,W)|^2, \tag{6}$$

$W = (E_K + \varepsilon)/(\frac{1}{2} Z^{*2})$, $Q_o = W^2/4\eta_K$, and $F_K(Q,W)$ is given by Khandelwal et al.[3] Tables of the function $f(\eta_K, \theta_K)$ or related quantities are available[3,4] from which target K-vacancy production cross sections can be calculated. With relativistic ions, one must calculate η_K using the ion velocity β^2, not the ion energy $(\gamma-1)Mc^2$, where $\gamma^{-2} = 1 - \beta^2$, as is usually prescribed.[3,4,14] For low-Z projectile ionization, where hydrogenic wave functions and energies are valid, these tables can be used by taking $\theta_K = 1$ and $Z_x = Z_t$.

For high-Z ions and target atoms, one should use Dirac electronic 1s and continuum wave functions.[16] At low ion velocities, the use of Dirac wave functions is known to enhance high-Z K-shell ionization cross sections.[17] The factor r^{s-1} in the 1s and continuum wave functions gives a weak divergence at small r because s [$=(1-\alpha^2Z^2)^{1/2}$, $\alpha = 1/137.037$] is less than unity, which contracts the radial electronic density distribution. This contraction enhances the electronic momentum distribution at large momentum q. Since the ionization form factor is just the Fourier transform of the product of the 1s and continuum electronic wave functions, the form factor at large q is enhanced, leading to larger ionization cross sections. For the present high-velocity ions, however, the minimum momentum transfer $q_o \sim E_K/\beta c$ is small, so one can approximate the form factor with

$$F(q) \sim i\mathbf{q}\cdot\langle\varepsilon|\mathbf{r}|1s\rangle. \tag{7}$$

In this case, the size of the radial wave functions, proportional to the expectation value of the electron coordinate **r**, affects the magnitude of the form factor. Hence, the contraction of the relativistic wave functions leads to smaller ionization cross sections at large ion velocities.

K-shell ionization cross sections were calculated for Xe, Au, and U projectiles using the plane-wave Born formulation of Jamnik and Zupancic.[16] All multipoles up to $\ell=3$ were included. The ratios of cross sections calculated using Dirac wave functions and energies to those using nonrelativistic wave functions and energies are shown in Fig. 1 for 1s ionization, 1s-2s excitation, and 1s-2p excitation. The excitation cross sections are relevant to studies of projectile x-ray production, which are discussed in a later paper in this series. The use of relativistic electronic wave functions clearly gives smaller

ionization cross sections at high velocities. Part of this reduction is due to wave-function effects, but part is due to the use of the larger Dirac binding energies [$(1-s)mc^2$ = 132 keV for U] than nonrelativistic ones [$Z^2/2$ a.u. = 115 keV for U]. The dipole 1s-2p excitation cross sections tend to be more reduced than the monopole 1s-2s ones. Dipole 1s ionization is dominant, but all multipoles up to $\ell=3$ contribute to the total ionization cross section. At small β, the relativistic cross sections increase, consistent with earlier calculations.[17]

C. Distortion Effects

For the high-Z targets and high-Z projectile ions used, the increased binding of the 1s electron and/or the polarization of the inner-shell wave functions affect the K-shell ionization cross sections.[7-10] At low velocities, where the target and projectile electrons form molecular orbitals, the increased binding of the 1s electron makes it more difficult to excite the electron, which gives smaller ionization cross sections.[7,10] At high velocities, molecular orbitals may not be formed, but the electron clouds are nevertheless strongly distorted by the perturbing potential. Since the potential is attractive, the electronic density is redistributed toward the perturbing nucleus, bringing the electron and perturber closer together, and increasing the probability of excitation.[8] For the relevant intermediate velocities ($v \sim v_K$), Basbas et al.[9] have developed a formulation that interpolates between the low- and high-velocity regimes. At the heart of the theory a cut-off impact parameter $b_c = c_K a_K$ (a_K is the Bohr radius of active electron, and c_K is a constant) is assumed, below which binding effects are dominant and above which polarization effects dominate. At low velocities, ionization occurs mainly at

impact parameters $b<a_K$, so binding effects should give reduced cross sections. At high velocities, ionization can occur at large impact parameters $b>a_K$, so the polarization effect gives increased cross sections. By changing the cut-off impact parameter, one changes the relative weighting of the binding and polarization effects. A value of $c_K = 1.5$ was chosen in Ref. 9 to fit existing experimental target-atom ionization data. The measurements described in the following section suggest the need to use a larger value of c_K for projectile ionization for large perturbing charges, thus deemphasizing the polarization effect. However, the expressions for binding and polarization effects developed in Ref. 9 are valid strictly only in the region of small perturbations, $Z_p << Z_t$ for target ionization or $Z_t << Z_p$ for projectile ionization. In some of the present cases, where Z_p is approximately equal to Z_t, the applicablilty of this theory is no longer certain.

D. Relativistic-Velocity Effects

Most of the effects discussed in Sects. II.A to C occur for nonrelativistic projectiles with energies less than about 20-MeV/amu. At relativistic velocities, the perturbing Hamiltonian consists of the Coulomb interaction between the perturbing nucleus and electron and, in addition, a magnetic current-current interaction. The longitudinal part of the current-current interaction combines coherently with the Coulomb potential to give the cross section calculated with the nonrelativistic PWBA.[5] The transverse interaction between the current of the perturbing nucleus $Z_x e\vec{\beta}c$ and that of the electron $e\vec{\alpha}$ gives a cross section that increases as $\ln\gamma^2-\beta^2$ at large projectile kinetic energies $(\gamma-1)Mc^2$. At high energies, the longitudinal part is constant, since it only depends on the ion velocity, which approaches a constant c. In the present

cases, where $\gamma \lesssim 1.2$, the transverse contribution increases the ionization cross sections by less than 4%. For high-Z target and projectile ionization, the transverse contribution should be calculated using Dirac wave functions (and including distortion effects), but because of the negligible magnitude of the transverse cross sections, the contributions were calculated with just the first-order plane-wave Born approximation.

E. Screening Effects

For projectile ionization by neutral target atoms, one must account for the screening of the perturbing nucleus by the target electrons.[6,18-20] This effect does not occur for target K-shell ionization by nearly bare projectiles. Paper II showed that the target screening reduced ionization and excitation cross sections for low-Z projectiles by significant factors. The transverse cross sections were so much more reduced than the longitudinal ones, that they could be neglected for low-Z projectiles with $E_p \lesssim 2000$-MeV/amu.

To account for electronic screening on projectile ionization, Eq. (3) has to be modified:[6,18]

$$\sigma_{1s} = \int_0^\infty d\varepsilon \int_{q_o}^\infty \frac{dq}{q^3} |F(q)|^2 \left[(Z_t - |F_t(q,Z_t)|)^2 + Z_t - \sum_{i=1}^{Z_t} |F_{it}(q,Z_t)|^2 \right], \quad (8)$$

where

$$F_{it}(q,Z_t) = \langle \psi_i | \exp(iq\cdot r) | \psi_i \rangle, \quad (9)$$

is the target form factor for the ith target electron occupying orbital ψ_i, $F_t = \Sigma_i F_{it}(q)$, and the sum is over all bound target electrons. The first term in the brackets in Eq.(8) is due to the normal perturbing potential represented by

Z_X^2 in Eq. (3). The screening correction $-|F_t(q,Z_t)|$ approaches Z_t at low q (corresponding to a fully screened potential) and vanishes at large q. The "antiscreening" term, Z_t, accounts for the ionization of projectile electrons by Z_t separate target electrons. The final term is an antiscreening correction factor that vanishes at large q and approaches Z_t at small q, cancelling out the antiscreening term.[6] The net effect of these terms is that for small q, corresponding to excitation at large impact parameters where the projectile would see a neutral target atom, the perturbing charge is nearly zero, but for large q, σ_{1s} varies as $Z_t^2+Z_t$, where Z_t^2 comes from the electron-target nucleus Coulomb potential and Z_t comes from Z_t separate electron-electron interactions.

For the present ~100-MeV/amu Xe ions, q is sufficiently large so that the calculated cross sections vary as $Z_t^2 + Z_t$. The binding and polarization effects affect the cross section term, proportional to Z_t^2, but not that associated with the Z_t separate electron-electron interactions. However, the theory of McGuire et al.[18] neglects kinetic-energy constraints on the electron contribution. In 82-MeV/amu Xe collisions, the target electrons have a kinetic energy of ~45 keV in the projectile frame, which is barely sufficient to ionize the Xe K shell electron (binding energy 42 keV). Therefore, this electron contribution ($Z_t\sigma_e$) is smaller than $Z_t\sigma_B$, where σ_B is the first Born cross section. We calculated this contribution using the formulas of Rudge and Schwartz[21] for electron-induced ionization cross sections σ_e, which agree reasonably well with experimental results near the threshold ionization energy.[22]

F. Experimental Effects

When one measures target K-vacancy production by bare projectiles, contributions due to the capture of target K electrons by the projectile are present[11] (as well as secondary processes discussed in paper I[1]). These contributions are difficult to estimate since one must calculate both the electron capture cross sections and the number of vacancies in the projectile into which the target electrons can be captured. Assuming equilibrium target thicknesses and that only zero-, one-, or two-electron projectiles are present, the capture contribution to target K-vacancy production is given by

$$\sigma_{K\text{capt}} = (\sigma_{KK} + \sigma_{KH})\, F_0 + (\tfrac{1}{2}\sigma_{KK} + \sigma_{KH})\, F_1 + \sigma_{KH}\, F_2 \,, \qquad (10)$$

where F_n is the measured equilibrium fraction of projectiles carrying n electrons, σ_{KK} is the capture cross section for single-electron capture from a fully occupied target K shell to an empty projectile K shell, and σ_{KH} is that where the electron goes into L-shell and higher projectile orbitals. Equation (10) assumes that the projectile is in its ground state (which is approximately valid for Xe projectiles used in this work, as shown in a later paper in this series). We included all charge fractions with n>2 in the n=2 fraction, since σ_{KH} is not significantly reduced by the presence of one or two 2s electrons (which only occurs for a small fraction of 82-MeV/amu Xe ions incident on high-Z targets).[2]

When one determines projectile ionization cross sections by passing one- or two-electron high-Z projectiles through a thin foil and measuring the zero- or one-electron fractions, capture and projectile excitation play no role. The target atom cannot capture projectile electrons efficiently due to the lack of bound state vacancies. For high-Z projectiles, excitation leads to the immediate radiative decay back to the ground state, because of the very short

lifetime of excited states compared to the time between ionizing collisions. Therefore, the projectile does not change charge unless 1s ionization occurs. We made numerical simulations for the present collisions using an 11-state model discussed in a later paper in this series, which includes excitation processes. As long as small target thicknesses are used, the simulations show that ionization cross sections measured using thin targets are exactly equal to the 1s ionization cross sections.

III. RESULTS

A. Projectile Ionization

In all the cases studied ~~that~~ the Xe^{52+} single-electron ionization cross section was equal to twice the Xe^{53+} ionization cross section within the experimental uncertainties shown in Figs. 2 to 4. To obtain the most accurate 1s single-electron ionization cross section, we took the weighted average of the measured Xe^{53+} and one-half of the Xe^{52+} single-electron ionization cross sections. From the linear target thickness dependence of the Xe^{54+} yield for a Xe^{52+} projectile, we could also search for two-electron ionization.

Figure 2 shows the single-electron and Xe^{52+} double-electron ionization cross sections for 200-MeV/amu projectiles. We discuss double-electron ionization in Sect. III.C. The solid lines in Fig. 2 were calculated using relativistic electronic wave functions and including transverse excitation and target screening effects, but not the wave-function distortion effects. The calculated cross sections increase roughly as Z_t^2. At low Z_t, the calculations are in good agreement with experiment, but are higher at large Z_t. We hypothesize that the discrepancy at large Z_t is due to distortion effects. To examine the wave-function distortion effects more carefully, we obtained

reduced cross sections using

$$\sigma_{red} = (\sigma_{meas} - Z_t\,\sigma_e)\,Z_t^{-2}\,, \tag{11}$$

where σ_{meas} are the measured cross sections, and $Z_t\sigma_e$ are the electron-induced contributions.

The theory of Basbas et al[9] with c_K=1.5 predicts that for these collisions, the reduced cross sections increase with Z_t, because the polarization effects are more important than binding effects (thin solid lines in Fig. 3). Clearly, this theory disagrees with the bulk of the high-Z_t data. To obtain better agreement, we semiempirically increased the cut-off impact parameter $b_c = c_K a_K$ to reduce the polarization effect and enhance the binding effect. Using c_K=3 brings the theory into better agreement with experiment (dashed lines in Figs. 2, 3 and 4). We found by trial and error that no improvement is obtained with other values of c_K; the value c_K=3 gives the best overall compromise fit.

The theory of Basbas et al.[9] is usually applied to calculate target inner-shell vacancy production where $Z_x << Z$ ($Z_p << Z_t$). In near-symmetric collisions at the present relativistic velocities ($v/v_K \sim 1$), a large number of theories have been developed to calculate ionization in H^++H collisions.[23,24] We can obtain reduced cross sections for Xe+Xe collisions by interpolating between measurements for Z_t = 47 and 79. By plotting $Z^2\sigma$ ($Z = Z_t = Z_p$) versus the proton kinetic energy, we can then compare Xe+Xe with p+H ionzation cross sections[25,26] at the same value of v/v_K. The Xe energy scale in Fig.4 is related to the p+H one using

$$E_{Xe} = 932\left[\frac{1}{\sqrt{1-\beta^2}} - 1\right];\quad \beta = \frac{54}{137.037}\sqrt{0.04025E_p}, \tag{12}$$

where E_{Xe} is in MeV/amu and E_p is the proton energy in keV. The Xe energy

scale ends at E_p = 160 keV where β approaches unity. This type of scaling is exact for symmetric collisions ($Z=Z_x$) in the PWBA[3] and in molecular perturbed stationary-state calculations for one-electron systems.[27] Since the target electron anti-screening effects have been removed in deriving the reduced cross sections, and the electronic relativistic effects and transverse excitation are negligible, this scaling should be nearly exact in the present Xe+Xe collisions. The measured Xe+Xe points are clearly in good agreement with the measurements of Shah and Gilbody[25] and Park.[26] We also show in Fig.4 the Basbas calculations using c_K = 1.5 (thin-solid line) and c_K = 3 (dashed line). Those using c_K = 3 are in reasonable agreement with the measured p+H and Xe+Xe cross sections, but the original theory with c_K = 1.5 significantly overestimates the p+H cross sections.

Of the many theories that have been developed to calculate ionization in p+H collisions, that giving the overall best agreement with experiment is probably the Glauber approximation. (See Park[23] and McGuire[24] for further comparisons.) One of the main things the Glauber approximation[24,28] for 1s ionzation does is that the unitarity of the ionization amplitude is preserved. For symmetric collisions near $v\text{-}v_K$, the first-order semiclassical approximation[14] predicts ionization probabilities that are greater than 1/2 in small-impact-parameter collisions. Such large probabilities deplete the initial 1s occupation amplitude $a_o(t)$, assumed to be unity for all times t in first-order theories like the PWBA, thus leading to smaller ionization probabilities and cross sections. It is not clear how the physical ideas behind this approximation can be compared with the physical ideas of binding and polarization in the theory of Basbas et al.[9]

Figure 3 compares Glauber calculations of the reduced ionization cross sections with experiment (chain curve). The Glauber theory agrees well with experiment (and with our emipirical modification of the theory of Basbas et al.[9] using $c_K = 3$) for $Z_t > 20$. The main disagreement occurs for $Z_t<20$, where the data points are higher than the Born calculations. The Glauber cross sections always lie below the Born ones, possibly indicating the lack of elements in the theory that can be physically connected with the polarization effect. The present low-Z_t data points do not agree with the original Basbas theory either. These points are most affected by target antiscreening. If the full Born electron-electron contribution $Z_t\sigma_B$ were subtracted from the measured cross sections instead of $Z_t\sigma_e$ (σ_e incorporating threshold effects), the reduced cross sections would be in better agreement with the Born and Glauber calculations at low Z_t (e.g. the 82-MeV/amu Xe+Be reduced cross sections are reduced by 25%). These considerations suggest the possibility that the discrepancy at low Z_t may be due to our lack of a complete theory of target screening and antiscreening near the electron ionization threshold velocity.

B. Target Ionization

Figure 5 compares the Basbas theory[9] to measurements of target K-vacancy production by 82- and 197-MeV/amu Xe ions. The cross sections for fixed projectile charge and velocity fall off rapidly with Z_t between Ni and U. In order to plot the cross sections on a linear scale comparable to Fig. 3, we multiplied the K-vacancy production cross sections by $(Z_t/Z_p)^4$. The resulting cross sections have a peak at the value of Z_t where the ion velocity is equal to the target K-electron velocity ($Z_t = 54$ at 82 MeV/amu and $Z_t = 77$ at 197 MeV/amu). This peak approximately reflects the peak seen at $\eta_K=1$ [Eq.(5)] in reduced ionization cross sections plotted against η_K (η_K increases from right to

left in Fig. 5 however).[15,29] The capture contributions were calculated using measured equilibrium fractions and the eikonal theory of nonradiative capture.[2] The solid and dashed lines in Fig. 4 were calculated using c_K=1.5 and 3, respectively, and include the capture contribution (shown as dash-dot lines). For target K-vacancy production, the experimental results lie closer to the original theory of Basbas et al[9] with c_K=1.5, except at low Z_t.

In principle, a theory of the binding and polarization effects should consistently predict target and projectile ionization cross sections; one should not be required to use a different cut-off impact parameter for the two different cases. Target-nucleus screening effects on the distortion effects on projectile ionization may differ from those on target ionization, but our calculations show that screening is negligible at high perturbing charge. We are not prepared to conclude that a discrepancy exists between the results for projectile and target ionization though. We estimate that the theoretical capture cross sections in Fig.5 are uncertain within a factor of two.[2] If the capture cross sections were doubled, the Basbas theory using c_K = 3 would fit the data better. Also, the independent electron theory used to calculate the capture contribution, Eq.(10), neglects processes like the capture of target L electrons followed by target K to L excitation, which may contribute significantly to the measured target K-vacancy production cross sections.[30]

C. Double Ionization

In the independent-electron approximation,[13] the probability of simultaneously ionizing two 1s electrons in a collision with impact parameter b is just the square of the single-electron ionization probability P(b) (per electron). In the semiclassical approximation the double-ionization cross section is given by

$$\sigma(1s^2) = \int_0^\infty 2\pi b db\, P^2(b). \tag{13}$$

Using SCA tables of the reduced impact parameter dependence of P(b),[14] the ratio of the double ionization cross section to the single ionization one is given by

$$\frac{\sigma(1s^2)}{\sigma(1s)} = D\,\frac{Z_t^2}{Z_p^2}, \tag{14}$$

where D is equal to 0.36, 0.30, and 0.26 for 82-, 140-, and 200-MeV/amu Xe projectiles.

The semiclassical calculations of Hansteen et al[14] are, like the plane-wave Born approximation ones, based on first-order perturbation theory. Target screening, transverse excitation, and Dirac-wave-function effects should not affect the ratio of the double ionization to single ionization cross sections significantly. Binding and polarization do affect the ratio, however, since the ionization probability at every impact parameter is reduced.[23] Since the constant D can be viewed as the average value of the ionization probability over the range of impact parameters contributing to the ionization cross section, a reduction of the probability at every impact parameter b due to distortion effects, should reduce the ratio of double ionization to single ionization. The lower limit to this reduction is the ratio of the single-ionization cross section calculated with binding and polarization to that without this correction (σ_{red}/σ_B in Fig.3). The application of this reduction factor gives the dashed curves in Fig. 2.

For $Z_t \lesssim 30$ in 200-MeV/amu Xe collisions, only an upper limit to the measured double ionization cross sections could be obtained. The data for Ag and Au targets are in agreement, within large experimental uncertainties, with the

theory including the distortion effects.

It would be desirable to increase the accuracy of the double-ionization measurements, which was determined here by poor counting statistics due to a limited amount of counting time. The ratio of the double-ionization to single-ionization cross sections indirectly tests the validity of the semiclassical-approximation calculations of P(b) for relativistic heavy ions. It is presently technically not feasible to measure directly the impact parameter dependence of projectile ionization at the BEVALAC accelerator, so the double-ionization cross section is the only means available to obtain information about the impact parameter dependence of the ionization probability.

IV. CONCLUSIONS

Measurements of projectile ionization cross sections using one-electron, high-Z, nearly relativistic heavy ions represents the cleanest method of studying wave-function distortion effects at intermediate velocities ($v \approx v_K$). Uncertainties in target K x-ray measurements due to x-ray fluorescence yields, contributions of secondary processes, and of K-electron capture by the projectile are completely absent when one measures projectile charge-changing cross sections at small target thicknesses.

The most significant results of the present measurements are, that for the first time, one can probe diverse theories of ionization ranging from those that have been used exclusively in near-symmetric collisions like p+H to those where the perturbing charge Z_x is much less than Z. In particular, one can examine theories like that of Basbas et al.[9] that have previously been used only for $Z_x \ll Z$ to see whether they are applicable also if Z_x is approximately equal to Z. Likewise, one can test theories like the Glauber approximation in highly asymmetric collisions where $Z_x \ll Z$. Our measurements using Xe ions are for velocities where $v \sim v_K$, as is the case for ~25 keV protons. This region of Z_p and v is ideal because electronic relativistic effects are relatively unimportant, the required projectile velocity is not so relativistic that tranverse excitation is significant, and the momentum transfer is large enough that electronic screening of the perturbing target nucleus is nearly negligible. In this region, the scaled Xe+Xe cross sections agree well with p+H ones.

The present results for projectile K-shell ionization suggest that the Basbas theory with $c_K = 1.5$ underestimates the binding effect at large perturbing charges. A larger binding-polarization cut-off impact parameter is

needed for projectile ionization, which is inconsistent with the present and many other measurements of target K-shell ionization, but is consistent with p+H ionization. The fact that the binding effect is underestimated or the polarization effect is overestimated at large Z_X may be due to the breakdown of the theory at large perturbing charge. The theory frequently truncates terms in Z_X beyond second order. Possibly the truncated higher-order terms for the binding effect outweigh those for the polarization effect. Possibly, the apparent good agreement between target ionization at nonrelativistic velocities and the original theory of Basbas et al.[9] is due to inaccurate estimates of target electron capture contributions.

The present evidence of projectile double-electron ionization is reasonably consistent with calculations in the independent-electron approximation.

ACKNOWLEDGEMENTS

This work was supported in part by the National Science Foundation Grant No. PHY-83-13676 (Stanford), by the Director; Office of Energy Research, Division of Nuclear Physics of the Office of High Energy and Nuclear Physics of the U. S. Department of Energy under Contract No. DE-AC03-76SF00098 (LBL), and by the U.S. Department of Energy contract No. DE-AC02-76CH00016 (BNL). We are indebted to Jim McGuire for making Glauber calculations of 1s ionization, shown in Fig.3.

References

1. R.Anholt, W.E.Meyerhof, Ch.Stoller, E.Morenzoni, S.A.Andriamonje, J.D.Molitoris, O.K.Baker, D.H.H.Hoffmann, H.Bowman, J.-S. Xu, Z.-Z. Xu, K.Frankel, D.Murphy, K.Crowe, and J.O.Rasmussen, Phys. Rev. A30, 2234 (1984) (paper I).

2. W.E.Meyerhof, R.Anholt, J.Eichler, H.Gould, Ch.Munger, J.Alonso, H.Wegner, and P.Thieberger, ms. submitted to Phys. Rev A. (paper III).

3. G.W.Khandelwal, B.H.Choi, and E. Merzbacher, At. Data 1, 103 (1969).

4. R.Rice, G.Basbas, and F.D.McDaniel, At. Data Nucl. Data Tab. 20, 503 (1977); O. Benka and A. Kropf, At. Data Nucl. Data Tab. 22, 219 (1978).

5. R.Anholt, Phys. Rev. A19, 1009 (1979).

6. R.Anholt, Phys. Rev. A31, 3579 (1985) (paper II).

7. W.Brandt, R.Laubert, and I.Sellin, Phys. Lett. 21, 518, (1966).

8. G.Basbas, W.Brandt, and R.Laubert, Phys. Lett. 34A, 277 (1971).

9. G.Basbas, W.Brandt, and R. Laubert, Phys. Rev. A17 1655 (1978).

10. R.Anholt and W.E.Meyerhof, Phys. Rev. A16, 190 (1977).

11. G.Lapicki and F.D.McDaniel, Phys. Rev. A22, 1896 (1980).

12. R.Anholt and J.Eichler, Phys. Rev. A31, 3505 (1985); J. Eichler, Phys. Rev. A32, 112 (1985).

13. J.H.McGuire and L.Weaver, Phys. Rev. A16, 41 (1977).

14. J.M.Hansteen, O.M.Johnsen, and L.Kocbach, At. Data. Nucl. Data Tables, 15, 306 (1975).

15. E.Merzbacher and H.W.Lewis, in Corpuscles and Radiation, vol. 34 of Encyclopedia of Physics, ed. by S. Flügge (Springer, Berlin, 1958).

16. D.Jamnik and C.Zupancic, K. Dan. Vidensk. Selsk. Mat.-Fys. Medd. 31, No. 2 (1957).

17. P.A.Amundsen, L.Kocbach, and J.M. Hansteen, J.Phys. B9, L203 (1976).

18. J.H.McGuire, N.Stohterfoht and P.Simony, Phys. Rev. A24, 97 (1981).

19. D.R.Bates and G.W.Griffing, Proc. Phys. Soc. (London) A68, 90 (1955).

20. J.S.Briggs and K.Taulbjerg in Structure and Collisions of Ions and Atoms, Vol. 5 of Topics in Current Physics, ed. by I.A.Sellin (Springer, New York, 1978), p. 105.

21. M.R.H.Rudge and S.D.Schwartz, Proc. Phys. Soc. London 88, 563 (1966).

22. C.J.Powell, Rev. Mod. Phys. 48, 33 (1976).

23. J.T. Park, Ad. At. and Mol. Physics 19, 67 (1983).

24. J.H. McGuire, Phys. Rev. A26, 143 (1982).

25. M.B. Shah and H.B. Gilbody, J. Phys. B14, 2361 (1981).

26. J.T. Park, private communnication. (The points in Fig. 4 are identical to those denoted Park (1980) in Fig.24 of ref.23.)

27. W. Thorson, Phys. Rev. A12, 1365 (1975).

28. J.E. Golden and J.H. McGuire, Phys. Rev. A15, 499 (1977).

29. J.D.Garcia, R.J.Fortner, and T.M.Kavanagh, Rev. Mod. Phys. 45, 111 (1973).

30. R.L. Becker, A.L. Ford, and J.F. Reading, J. Phys. B13, 4059 (1980).

31. J.U.Andersen, E.Laegsgaard, M.Lund, and C.D.Moak, Nucl. Inst. Methods 132, 507 (1976).

Figure Captions

Fig. 1. Ratios of 1s-2s and 1s-2p excitation and 1s-ionization cross sections for Xe, Au, and U projectiles calculated with Dirac relativistic wave functions and with nonrelativistic wave functions.

Fig. 2. Single-ionization 1s cross sections and double-ionization cross sections for Xe^{52+} ($1s^2$) plotted against target atomic number for 200-MeV/amu Xe. In the plane-wave Born approximation, the single-ionization cross sections increase as $Z_t^2 + Z_t$ (solid line). Wave-function distortion effects reduce the single-ionization cross sections (dashed lines). The computed double-ionization cross sections (solid lines) are a factor of 0.26 Z_T^2/Z_p^2 below the single-ionization ones (dashed lines). The distortion effects further reduce the double-ionization cross sections, as described in the text. The lower limit of this reduction on double ionization is shown by the dashed lines.

Fig. 3. Reduced projectile ionization cross sections for 81.5-, 140-, and 200-MeV/amu Xe ions plotted against target atomic number. The thick solid lines are PWBA calculations, and the thin solid lines were calculated with the theory of Basbas et al (Ref. 9) for binding and polarization effects using c_K = 1.5 and c_K = 3 (dashed lines). The chain curves are Glauber-approximation calculations.

Fig. 4. Scaled p+H and Xe+Xe 1s ionization cross sections plotted against proton kinetic energy. The PWBA (thick solid line), Basbas theory using c_K = 1.5 (thin solid line) and c_K = 3 (dashed line), and Glauber theory (chain curve) results are shown. The p+H data points are from Park[26] (triangles) and Shah and Gilbody[25] (closed circles). Some of Park's points for E_p>50 keV have been

omitted.

Fig. 5. Target K-vacancy production cross sections for 82- and 197-MeV/amu Xe projectiles, multiplied by $(Z_t/Z_p)^4$. The calculated capture contributions to the total K vacancy production cross section are shown by the chain curves. The solid and dashed lines were calculated using the Basbas theory of polarization and binding effects (Ref. 9) using c_K = 1.5 and 3 respectively and include the capture contributions.

TABLE 1

EFFECTS ON K-SHELL IONIZATION

Effect	On Target Ionization	On Projectile Ionization	
		Low-Z	High-Z
First order theory	PWBA	PWBA	PWBA
Electronic wavefunction	$\psi_o \sim e^{-Z^* r}$; use $Z^* = Z_t - 0.3$	$\psi_o \sim e^{-Zr}$; $Z = Z_p$	Dirac; $Z = Z_p$ $\psi_o \sim r^{s-1} e^{-Zr}$
Binding energy	$E_K = \theta_K \frac{1}{2} Z^{*2}$	$E_K = \frac{1}{2} Z^2$	$E_K = (1-s)mc^2$, $s^2 = 1 - \alpha^2 Z^2$
Wavefunction distortion	Polarization+ binding effect	$v/v_K > 10$ no correction	$v/v_K \sim 1$ to 2 corrections needed
Relativistic velocity $\vec{\beta} \cdot \vec{\alpha}$ interaction	calculate with Z^*, θ_K	negligible	calculate with Dirac wavefunctions
Perturbing nucleus screening	bare projectiles no screening	cross-section reductions	$Z_t^2 \rightarrow Z_t^2 + Z_t$
Coulomb deflection	negligible	negligible	negligible
Experimental effects	Target K-electron capture		

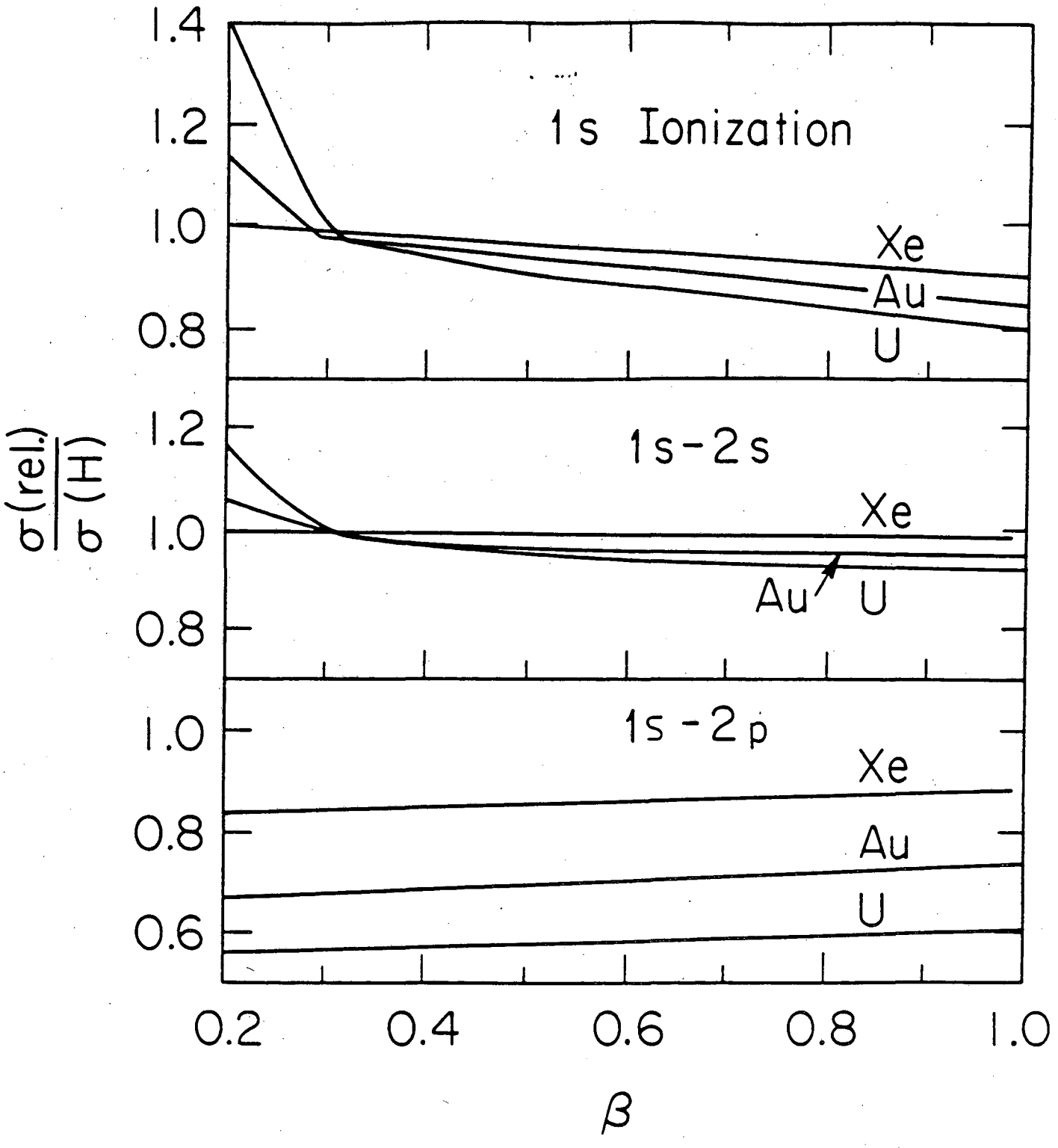
1.4
1.2
1.0
0.8
1s Ionization
Xe
Au
U
1.2
1.0
0.8
1s-2s
Xe
Au
U
1.0
0.8
0.6
1s-2p
Xe
Au
U
σ(rel.)/σ(H)
0.2
0.4
0.6
0.8
1.0
β

Fig. 1

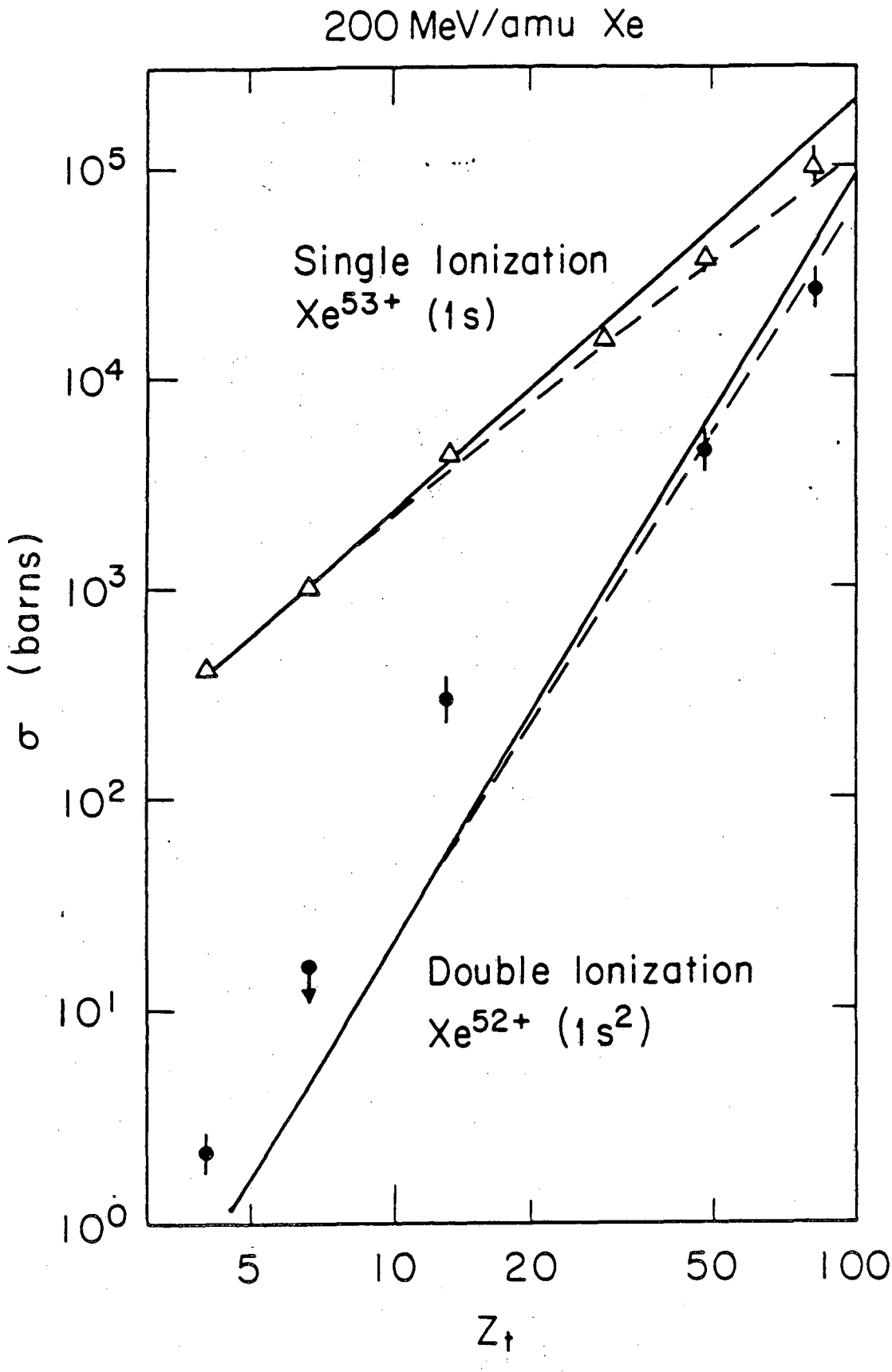
200 MeV/amu Xe
Single Ionization
Xe53+ (1s)
Double Ionization
Xe52+ (1s2)
σ (barns)
Zt
10^5
10^4
10^3
10^2
10^1
10^0
5
10
20
50
100

Fig. 2

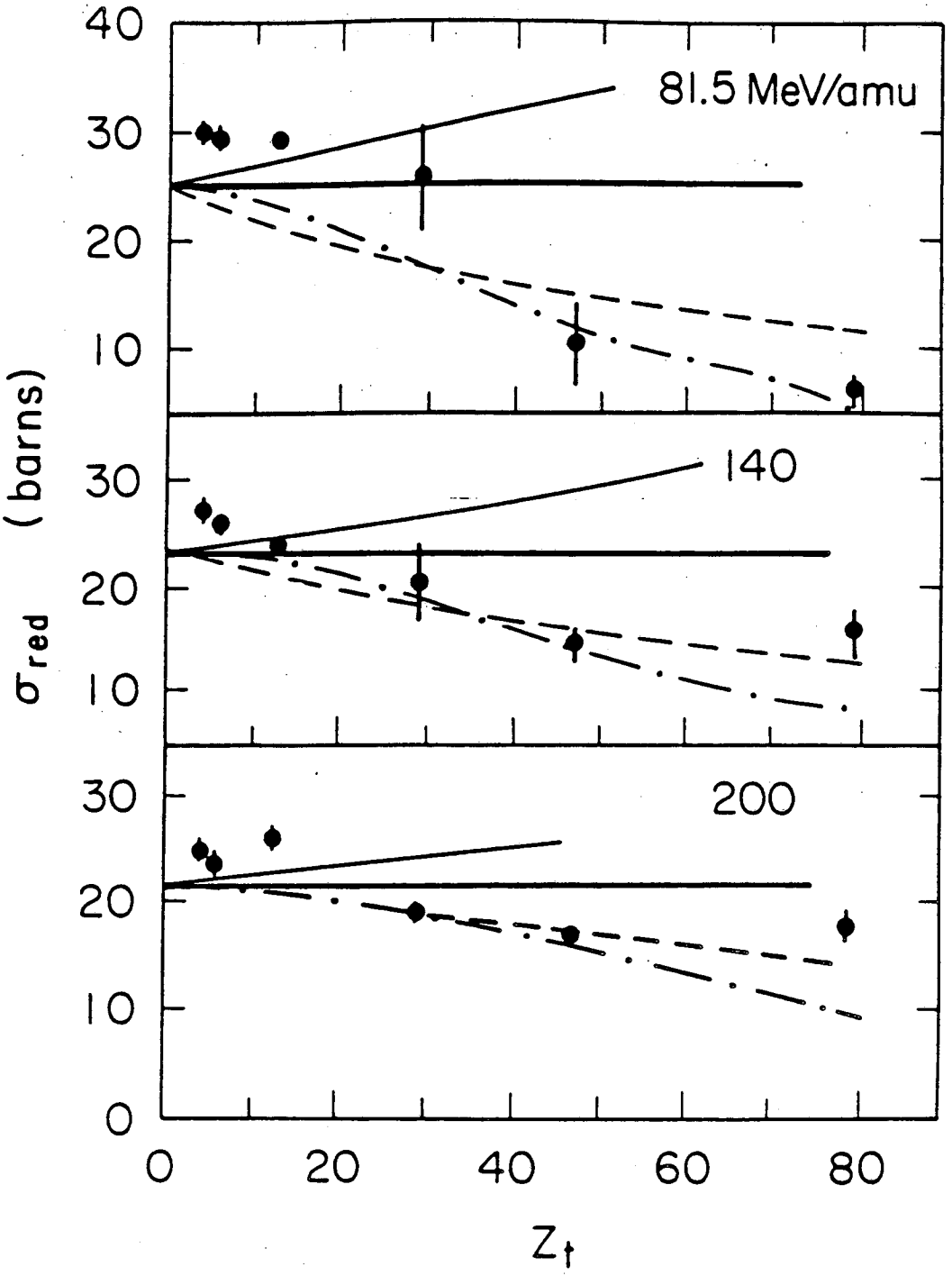

Fig. 3

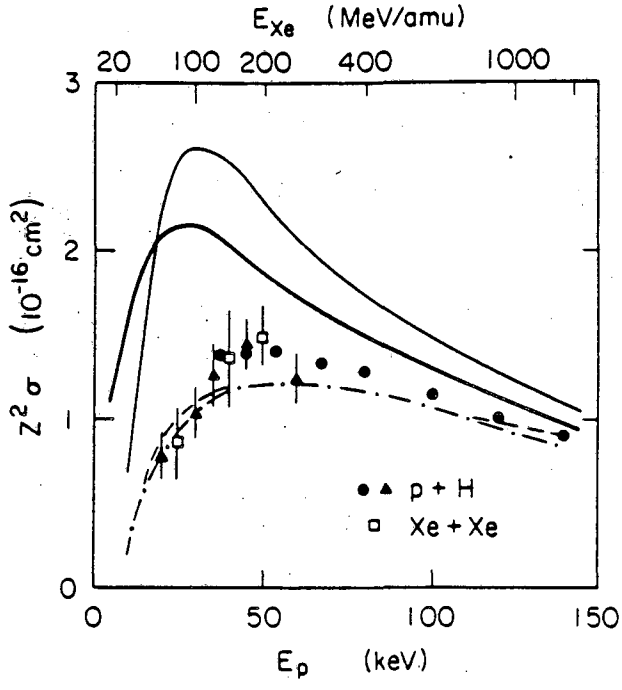
E_{Xe} (MeV/amu)
20
100
200
400
1000
3
2
1
0
$Z^2\sigma$ (10^{-16} cm^2)
● ▲ p + H
□ Xe + Xe
0
50
100
150
E_p (keV)

Fig. 4

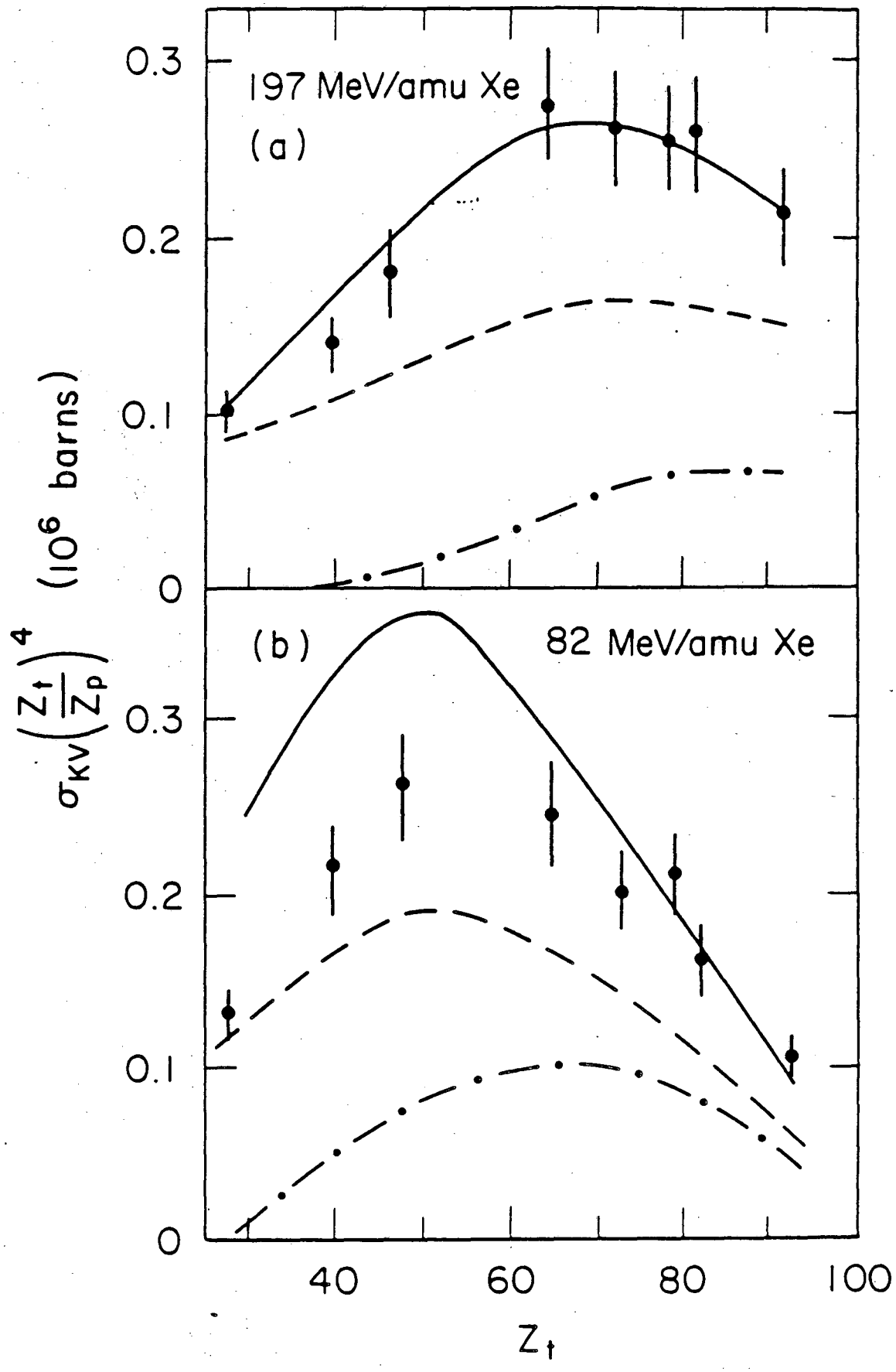
197 MeV/amu Xe
(a)
82 MeV/amu Xe
(b)
0.3
0.2
0.1
0
40
60
80
100
Z_t
$\sigma_{KV}\left(\frac{Z_t}{Z_p}\right)^4$ (10^6 barns)

Fig. 5

LAWRENCE BERKELEY LABORATORY
TECHNICAL INFORMATION DEPARTMENT
UNIVERSITY OF CALIFORNIA
BERKELEY, CALIFORNIA 94720